Bulletin of the Seismological Society of America, Vol. 96, No. 5, pp. 1827–1835, October 2006, doi: 10.1785/0120050260

Deconvolution of Three-Component Teleseismic *P* Waves Using the Autocorrelation of the *P* to *SV* Scattered Waves

by Saptarshi Dasgupta and Robert L. Nowack

Abstract The deconvolution of three-component teleseismic *P* waves is investigated using the autocorrelation of the *P* to *SV* scattered waves, which is important for improved imaging of crustal and upper mantle structure. The *SV* component of the *P* waveform is first estimated by transforming the three-component seismic data to the *P–SV–SH* frame of Kennett (1991) and also taking into account the free surface. This removes the direct *P* wave from the *SV* component leaving only the scattered *P* to *SV* waves. Assuming that the *P* to *SV* scattering coefficients are random and white, then the autocorrelation of the *SV* component provides an estimate of the autocorrelation of the source wavelet. This is analogous to the use of the autocorrelation of a reflection seismogram in exploration seismology to estimate the source pulse where the *P*-wave reflectivity is assumed to be random and white. A minimum-phase source wavelet estimated from the autocorrelation of the *SV* component can be used to deconvolve the unrotated radial and *Z* components that have been processed to be minimum phase. A minimum-phase source wavelet is not required, but the direct *P* wave must be larger than the scattered waves on the unrotated components. To enhance the direct wave, we use rotated coordinates about the direct *P*-arrival direction. This procedure is first tested on synthetic data and then applied to observed data from the 1993 Cascadia experiment where both *P* to *P* and *P* to *SV* scattered waves are estimated from the data that have been deconvolved using the autocorrelation of the *SV* component.

Introduction

We investigate an approach to deconvolve the vertical and radial components of teleseismic *P*-wave data using the autocorrelation function of the transformed *SV* component. In the traditional receiver function approach, the vertical component is used as an approximate estimate of the source wavelet to deconvolve the radial component (Vinnik, 1977; Langston, 1977, 1979; Owens *et al.*, 1984). The emphasis in the receiver function approach is *P–SV* scattering and not *P–P* scattering. An alternate approach was used by Bostock (2004), who attempted to separate the source time function from the scattered teleseismic data by using spectral properties of the signal. A multichannel deconvolution technique for the transformed minimum-phase *P* seismograms was used with constraints to deconvolve the seismic data. Baig *et al.* (2005) used the cross correlogram of two seismogram components to estimate the spectrum of the source wavelet, and Mercier *et al.* (2006) used the approach to obtain estimates of *P*-component teleseismic-*P* Green's functions. Li and Nabelek (1999) compared three stacking techniques to enhance scattered waves from beneath the seismic array. In their approach, they estimated the stacked source wavelet and deconvolved it from the seismograms. Langston and Hammer (2001) also used stacking across the seismic array to estimate the source wavelet.

In the approach followed here, simultaneous estimation of the source wavelet and the Earth structure is investigated on the assumption that the structural response is white. First the data is transformed to form the *P–SV–SH* components incorporating the effect of the free surface. Assuming that the *P* to *SV* scattering coefficients are random and white, an estimate of the source wavelet is then obtained from the autocorrelation of the *SV* component of the three-component teleseismic data. This is similar to the deconvolution process used in exploration seismology where the *P* reflectivity is assumed to be random and white (Webster, 1978; Robinson and Osman, 1996). In contrast to the use of reflected waves in exploration, we don't require the source wavelet from the earthquake to be minimum phase but only assume that the directly transmitted wave is larger than the scattered waves. For the observed data, we use a rotation to vectors 45° from the direction of the direct *P* wave to ensure that the direct wave is sufficiently large on these components. Before deconvolution these processed components are then rotated back to the vertical and radial components.

The *SV* autocorrelation method is first tested using a one-dimensional (1D) model for a random scattering series and then a two-dimensional (2D) collisional suture model. The method is then applied to teleseismic data from the 1993 Cascadia seismic experiment. In particular, the estimated source wavelet from the *SV* autocorrelation can be used to retrieve the scattered *P* to *P* reflectivity.

Description of the Method

We assume that the scattering coefficients from the subsurface are random and white. The seismic data are then the convolution of the source wavelet with the scattering coefficients. By transforming the components and using a free surface correction, the *SV* component is obtained removing the direct *P* wave from this component. Similarly, the *P* component can be obtained, which only includes the direct *P* and *P* to *P* scattered phases (Kennett, 1991; Reading *et al.*, 2003; Svenningsen and Jacobsen, 2004). However, Svenningsen and Jacobsen (2004) showed that for observed data the *P–SV–SH* transformation of Kennett (1991) is comparable to the *L–Q–T* rotated frame of Vinnik (1991) with the differences being small. The autocorrelation of the *SV* component provides an estimate of the autocorrelation of the source wavelet if the *P* to *SV* scattering coefficients are random and white. This is similar to using the autocorrelation of a reflection seismogram to estimate the source time function in exploration seismology. For the teleseismic case, the *SV* autocorrelation can be used to deconvolve the processed, unrotated components of the seismic data.

Assume first that the seismic *P* phases oriented in the direction of the incident *P* direction are made up of the direct *P* arrival represented by a delta function followed by random *P* to *P* scattering coefficients, $R_{P\_P}(t)$. Thus,

$$R_P(t) = \delta(t) + R_{P\_P}(t). \quad (1)$$

The scattered *SV* phases are transformed to include only *P* to *SV* scattering coefficients $R_{P\_SV}(t)$, and

$$R_{SV}(t) = R_{S\_SV}(t). \quad (2)$$

Now the transformed *P* and *SV* components are the result of the scattering time series $R_P(t)$ and $R_{SV}(t)$ being convolved with the source wavelet as

$$P(t) = S(t) * \{\delta(t) + R_{P\_P}(t)\} \quad (3)$$

$$SV(t) = S(t) * R_{P\_SV}(t), \quad (4)$$

where * indicates convolution.

The autocorrelation function of the *SV* component will be approximately equal to the autocorrelation function of the source wavelet if the autocorrelation of the scattering coefficients is random and white. Thus,

$$SV(t) * SV(-t) = \{S(t) * S(-t)\} * \{R_{P\_SV}(t) * R_{P\_SV}(-t)\} \sim S(t) * S(-t), \quad (5)$$

where $\{R_{P\_SV}(t) * R_{P\_SV}(-t)\} \sim \delta(t)$ for random and white *P* to *SV* scattering coefficients. This is similar to the assumption made for the deconvolution of reflection seismograms in exploration seismology where *P* to *P* scattering coefficients are assumed to be random and white (Webster, 1978; Robinson and Osman, 1996). The Fourier transform of the autocorrelation of the source wavelet is its power spectrum. Thus, the Fourier transform of $S(t) * S(-t)$ is $|S(\omega)|^2$ and the Fourier transform of $R_{P\_SV}(t) * R_{P\_SV}(-t)$ is approximately one for a random and white scattering series $R_{P\_SV}(t)$.

To form the complete source wavelet from the power spectrum, knowledge of the phase spectrum is necessary. For a minimum-phase signal, the log of the power spectrum and the phase spectrum form a Hilbert transform pair (Oppenheim and Schafer, 1975). We can therefore construct a minimum-phase source wavelet from the power spectrum and use it for the deconvolution. However, an earthquake source time function is not in general minimum phase. But the original seismic data can be processed to be minimum phase, and these processed data can be deconvolved with the estimated minimum phase source wavelet from the *SV* autocorrelation function. This assumes that the direct *P* is larger than the scattered waves on these components or in other words, the power spectrum of the direct pulse is greater at all frequencies than the residual time series that consists of the scattered phases.

For the transformed $P(t)$ component, the direct wave is included along with the *P* to *P* scattered phases. Following Bostock (2004), we assume that $\{\delta(t) + R_{P\_P}(t)\}$ is minimum phase for near vertically scattered waves from an incident teleseismic wave. Therefore, the scattered waves will all be smaller in amplitude than the direct wave for this component. For wide angle scattering, there could be exceptions to this, but here we are only interested in forward scattering for an incident wave in the near-vertical direction. For this case, the processed minimum-phase version of $P(t)$, $P_{\mathrm{MP}}(t)$ is just the minimum-phase version of the source wavelet $S_{\mathrm{MP}}(t)$ convolved with $\{\delta(t) + R_{P\_P}(t)\}$. Since the minimum-phase source wavelet $S_{\mathrm{MP}}(t)$ can be obtained from the autocorrelation of the *SV* component of the data, we can deconvolve $P_{\mathrm{MP}}(t)$ by $S_{\mathrm{MP}}(t)$ to find the scattering series $R_{P\_P}(t)$. To deconvolve other components of the teleseismic *P* wave, we rotate the original vertical and radial components to coordinates 45° from the direct *P* direction and then compute the minimum-phase signals. These are then rotated back to the vertical and radial components and deconvolved with the minimum-phase wavelet $S_{\mathrm{MP}}(t)$.

Application to Transmission Synthetic Data

The method described previously is first tested using a synthetic scattering series shown in Figure 1a. For the trans-

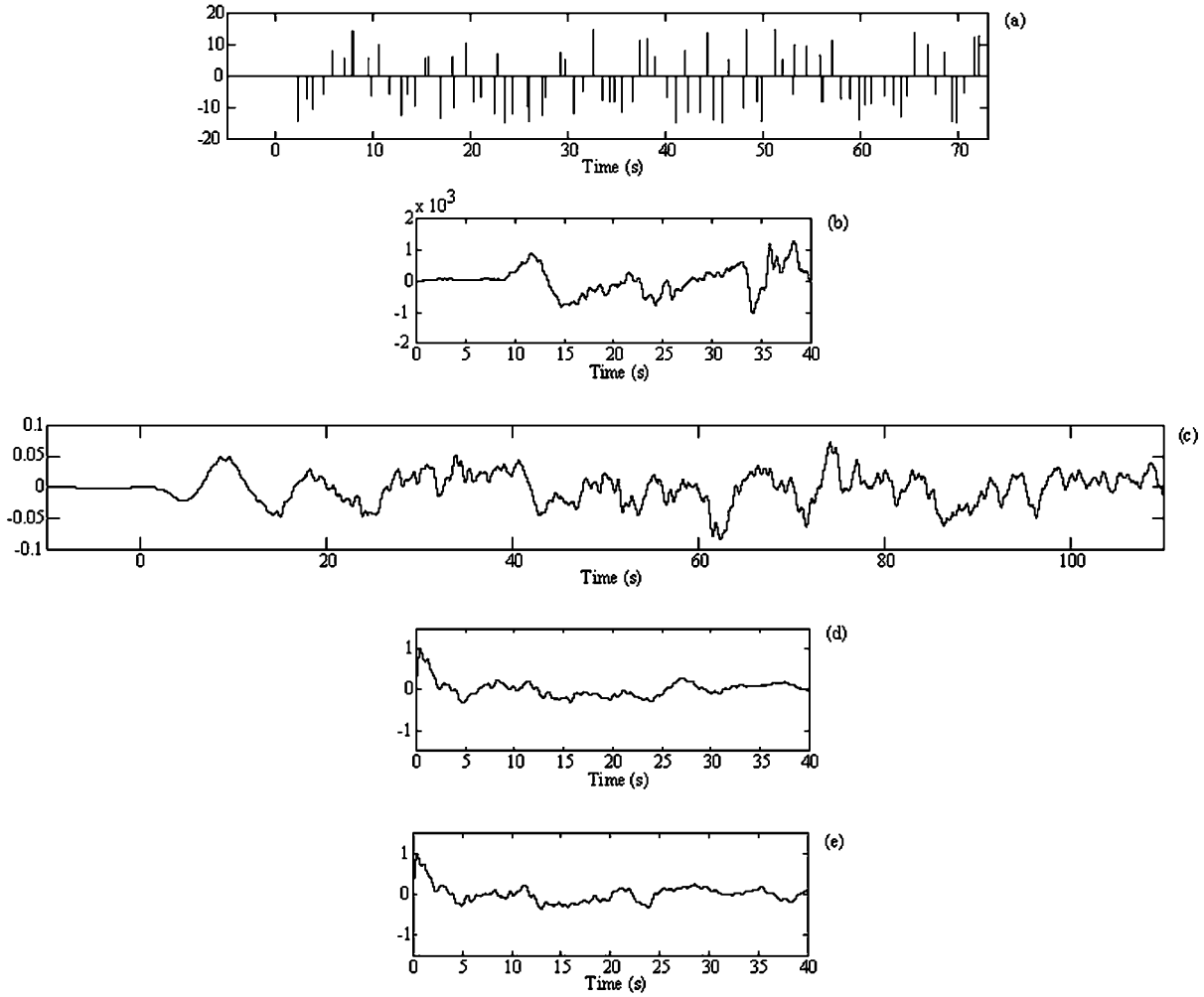

Figure 1. (a) The synthetic *P–SV* coefficients; (b) the source wavelet; (c) convolution of the synthetic *P–SV* coefficients and the source wavelet resulting in the synthetic *SV* seismogram; (d) the direct minimum-phase construction of the source wavelet in b; (e) estimate of the minimum-phase wavelet formed from the autocorrelation of the synthetic *SV* seismogram in c.

mission case, this would be from *P* to *SV* scattering. The scattering coefficients consist of 200 random located spikes with randomly varying amplitudes, where only the scattering coefficients in the first 72 sec are shown. The autocorrelation of the scattering series is approximately a delta function and its power spectrum is nearly white. Figure 1b shows the source wavelet that was used for this numerical test, which was derived from an observed *P*-waveform trace from the 1993 Cascadia seismic experiment. The source wavelet is about 40 sec long and has two distinct pulses with the later one being slightly larger, giving a non-minimum-phase wavelet. The convolution of the source wavelet and the scattering coefficients in Figure 1a is shown in Figure 1c. This is analogous to the *SV* component described previously.

Figure 1d shows the minimum-phase construction from the actual source wavelet in Figure 1b obtained using a Hilbert transform of the log of the power spectrum. Figure 1e shows the estimate of the source wavelet obtained by a minimum-phase construction from the autocorrelation of the *SV* wave. Although some of the details in the later parts of the traces in Figure 1d and e are different, the initial parts of the traces are very similar.

An initial impulse was added to the beginning of the scattering series to simulate the arrival of the transmitted *P*-wave phase, for example on a radial component. We call this impulse a replicator since it has the effect of reproducing the scattering series in the autocorrelation function. The convolution of the source wavelet with the combined direct wave impulse and the scattering coefficients is used to form the synthetic transmission seismogram shown in Figure 2a. Figure 2b shows the synthetic transmission seismogram processed to be minimum phase. Figure 2c displays the result of the deconvolution of the transmission seismogram processed to be minimum phase with the estimate of the minimum source wavelet from the *SV* autocorrelation function in Figure 1e. Figure 2d is the original scattering series with

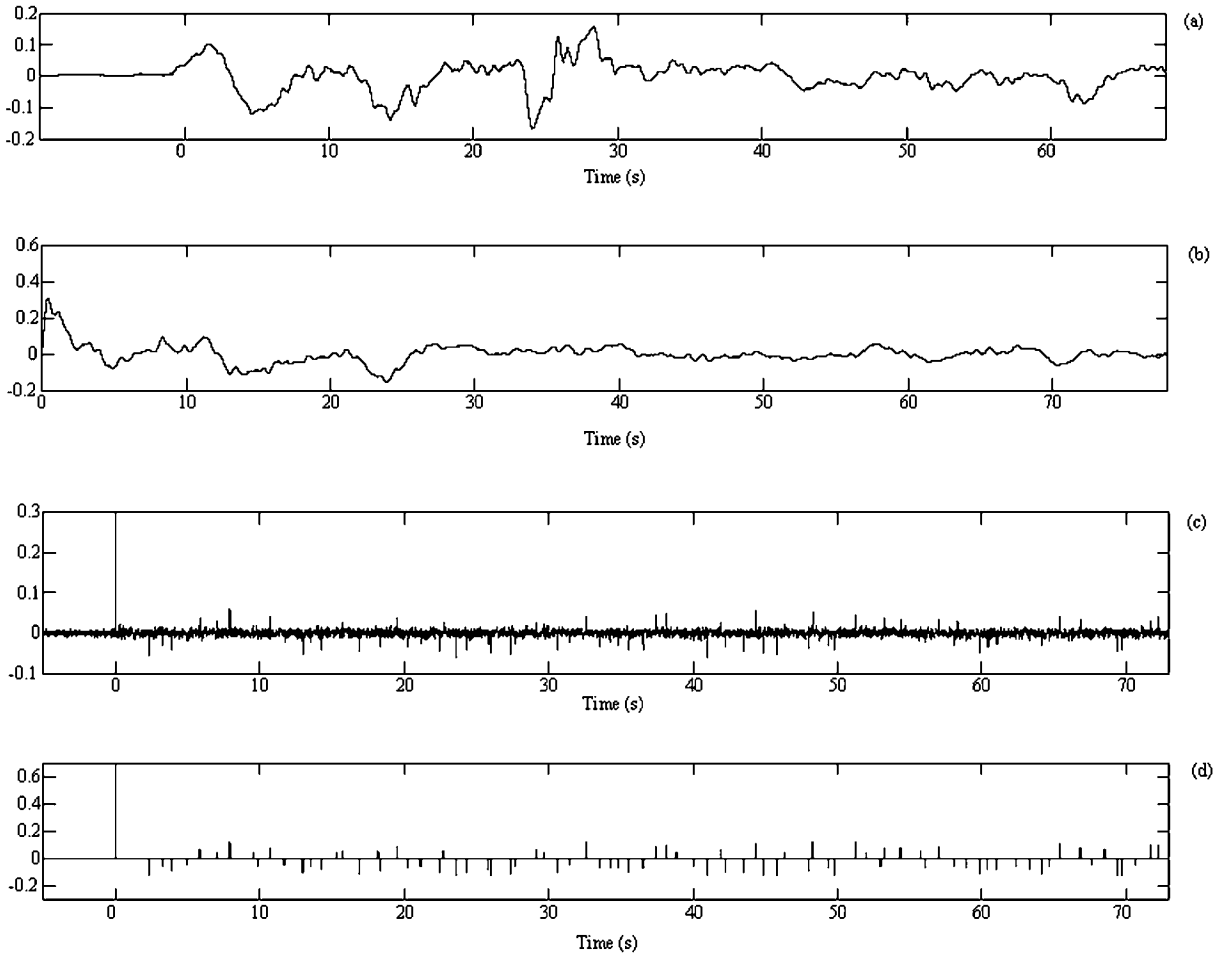

Figure 2. (a) Convolution of the combined direct-wave impulse and the *P–SV* coefficients in d with the source wavelet in Figure 1b; (b) minimum-phase construction of the synthetic transmission seismogram; (c) the combined impulse plus *P–SV* coefficients reconstructed with the estimate of the minimum-phase source wavelet in Figure 1e; (d) true *P-SV* scattering coefficients with direct-wave impulse.

the direct-wave impulse and can be compared with the deconvolution estimate in Figure 2c. The result shows that the reconstructed scatterers match up very well with the known scatterers. However, the deconvolution results are sensitive to the water table used, as well as to the size of the impulse replicator. Here we have used a water table of 0.00002 to avoid division by zero for spectral holes in the deconvolution. We have also used an impulse replicator of about 8 times larger than the scattering amplitudes. Nonetheless, this example illustrates the use of the *SV* autocorrelation for deconvolution.

We performed a second test of the method using 2D synthetics computed using a collisional suture model, which has been described in more detail in Nowack *et al.* (2006). Figure 3a shows the synthetic radial seismograms for the collisional suture model. Figure 3b shows an observed trace from the 1993 Cascadia seismic experiment used as a source wavelet and is the same source wavelet used in the 1D example. Figure 3c shows the result of the radial component convolved with the source pulse. Figure 3d shows the deconvolved radial seismograms obtained after deconvolution using the *SV* autocorrelation in which the *SV* component was approximated by not including the direct-wave impulse. Although these traces were not random, a reasonably good deconvolution can still be obtained. For stability we applied a bandpass filter (0.1–0.5 Hz) to the deconvolution results.

Application to Teleseismic Cascadia Data

The method described previously has been applied to several teleseismic events recorded in Oregon as part of the 1993 Cascadia seismic experiment (Li and Nabelek, 1999; Bostock *et al.*, 2001; Rondenay *et al.*, 2001; Shragge *et al.*, 2001). During the experiment a linear array was deployed perpendicular to the coast of Oregon (Fig. 4). The earthquakes considered here include one in Argentina (seismic event 5 from Rondenay *et al.*, 2001), one north of New Guinea (seismic event 14 from Rondenay *et al.*, 2001) and

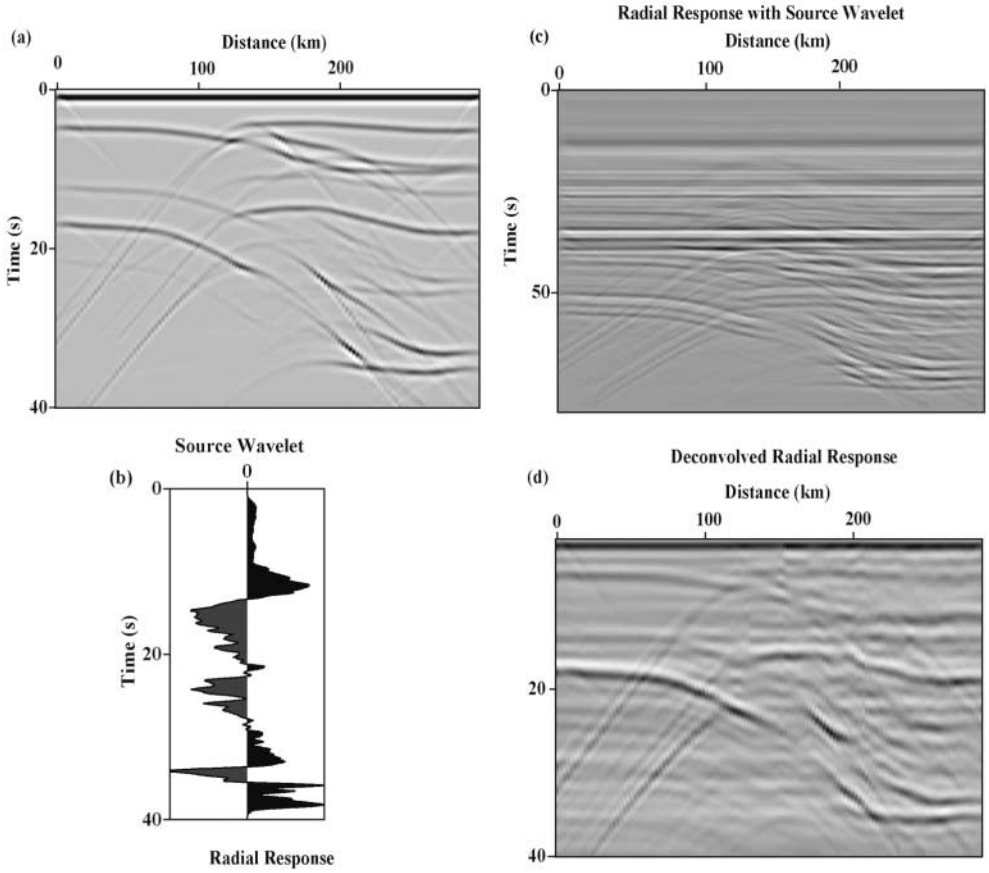

Figure 3. (a) The radial response of the collisional suture model; (b) the source wavelet; (c) the convolution of the radial response with the source wavelet; (d) the deconvolved radial response using the *SV* autocorrelation approach.

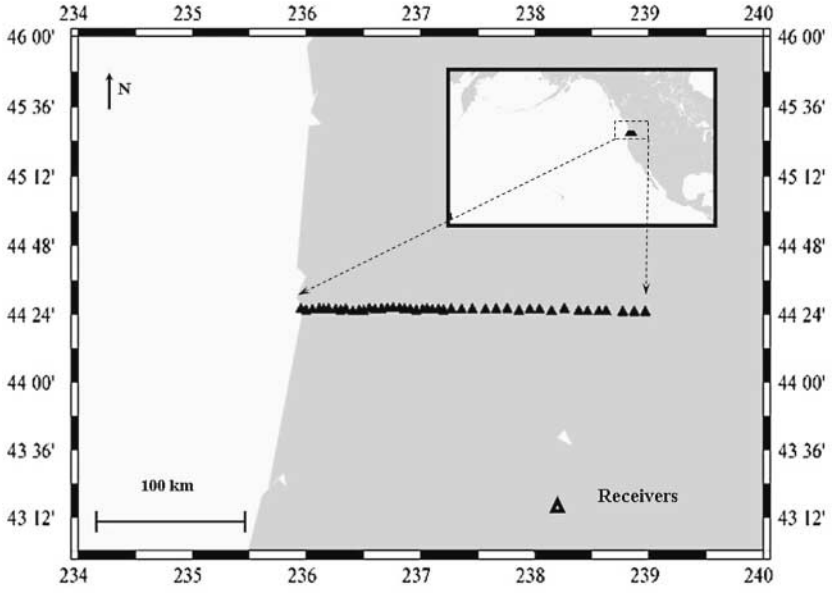

Figure 4. Location and orientation of the seismic stations from the 1993 Cascadia seismic experiment.

one in Mexico (seismic event 15 from Rondenay *et al.*, 2001). For individual stations from each event, the original vertical, north–south, and east–west components were transformed into the *Z–R–T* geometry. The **Z–R** components in the plane of incidence were further processed to obtain the *P–SV* seismograms accounting for the free surface (Kennett, 1991; Reading *et al.*, 2003; Svenningsen and Jacobsen, 2004). These transformations are illustrated in Figure 5 for seismic event 16. The transformation of the *Z* component to the *P* component is shown in Figure 5a. Figure 5b shows the transformation of the *R* component to the *SV* component. Note that the direct *P* wave has been removed from the *SV* component.

From the 1D synthetics presented earlier, we found that the amplitude of the direct wave in relation to the scattering amplitudes was an important parameter for the deconvolution. Thus, we transformed the **Z–R** vectors to rotated **w1–w2** vectors 45° from the direct *P* direction. This transformation will enhance the direct *P* phase on these components as shown in Figure 6 for station A10 for seismic event 16. The **w1–w2** vector pair is then processed to be minimum phase and transformed back to the **Z–R** geometry to obtain the minimum phase reconstruction of the *Z* and *R* components as shown in Figure 7.

Figure 8 shows deconvolved radial traces from four stations for seismic event 15 comparing the deconvolution results using the *SV* autocorrelation approach and the receiver function method. The arrows show the approximate location of the *PpPs* phases from the slab structure identified by Rondenay *et al.* (2001). The traces have been filtered with a zero phase, low-pass butterworth filter with a corner of 0.3 Hz.

Figure 9 is an image plot of the traces for seismic event 14 for the radial components deconvolved with the *SV* autocorrelation approach. We used the same water level of 0.00002 for all traces to avoid division by zero for spectral holes in the deconvolution. The first half of the traces had a 4-km spacing and the other half was at 8-km spacing. They have been interpolated to an equal spacing of 4 km prior to making the image plots using Seismic Unix, (SU) (Stockwell and Cohen, 2002). Also, the direct *P* has been muted out at about 18 sec. The result shows the deconvolution of the minimum-phase radial seismograms with the minimum-

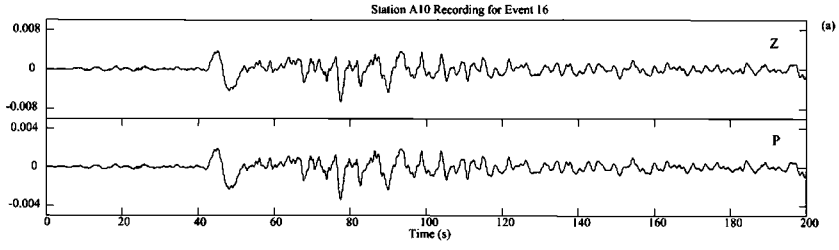

Figure 5. (a) The *Z* component is transformed to the *P* component for station A10 from seismic event 16 using the transformation of Kennett (1991) and Svenningsen and Jacobsen (2004); (b) the *R* component transformed to the *SV* component for station A10 for seismic event 16. Note that the direct *P* wave has been removed from the *SV* component.

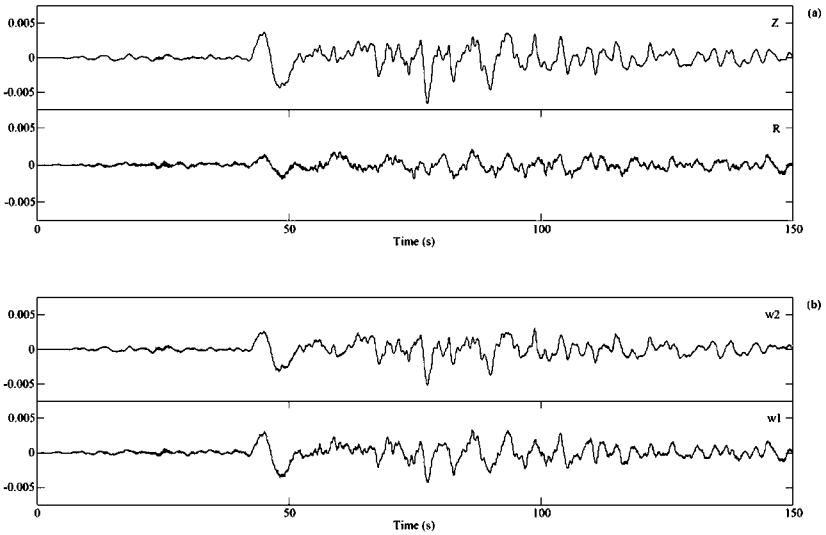

Figure 6. (a) The **Z–R** vectors of station A10 for seismic event 16; (b) The vectors **w1** and **w2** obtained after rotation for station A10 of seismic event 16.

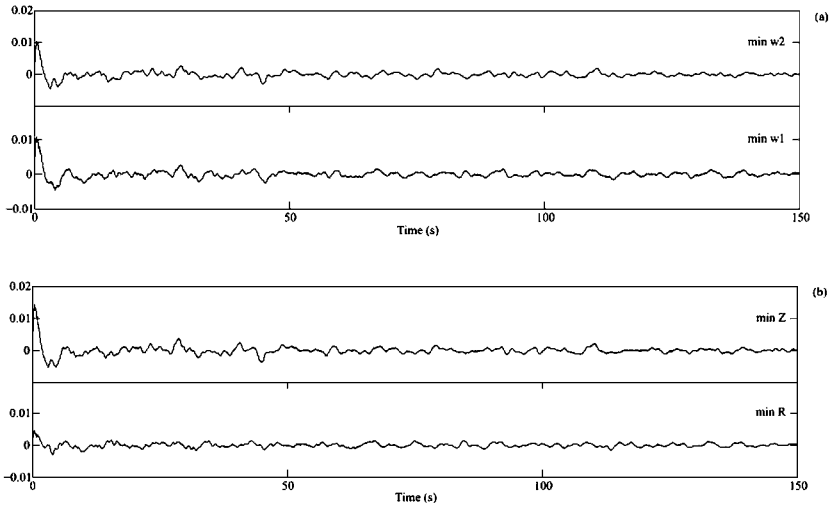

Figure 7. (a) The minimum-phase-processed **w1** and **w2** vectors; (b) the rotated minimum-phase-processed vectors rotated back to the *Z* and *R* components for station A10 for event 16 from Rondenay *et al.* (2001).

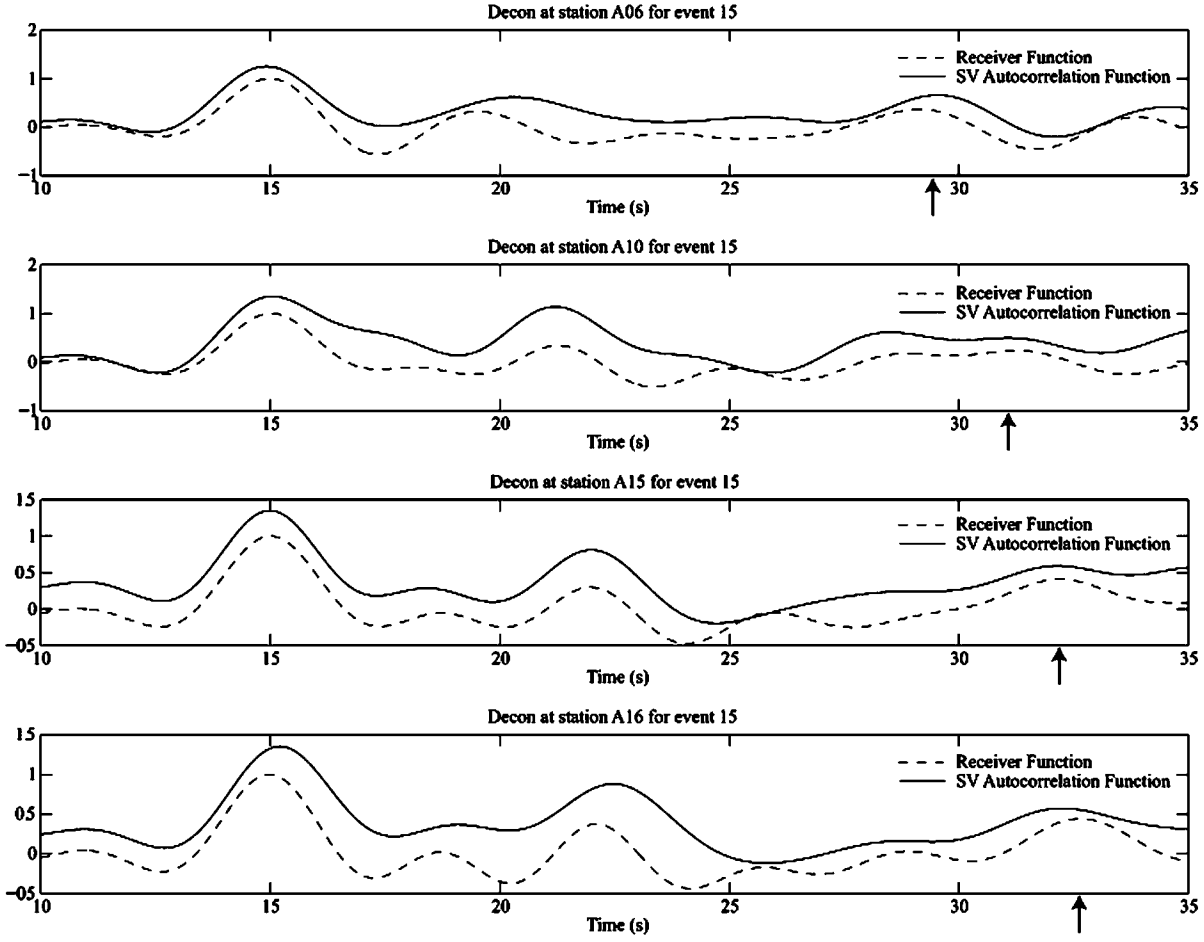

Figure 8. Comparisons of the deconvolved radial seismograms from the *SV* autocorrelation approach and the receiver function method. The comparisons show several stations from seismic event 15 of the 1993 Cascadia seismic experiment. The seismograms have been filtered using a zero-phase butterworth filter to be less than 0.3 Hz. The arrows show the approximate location of the *PpPs* phases.

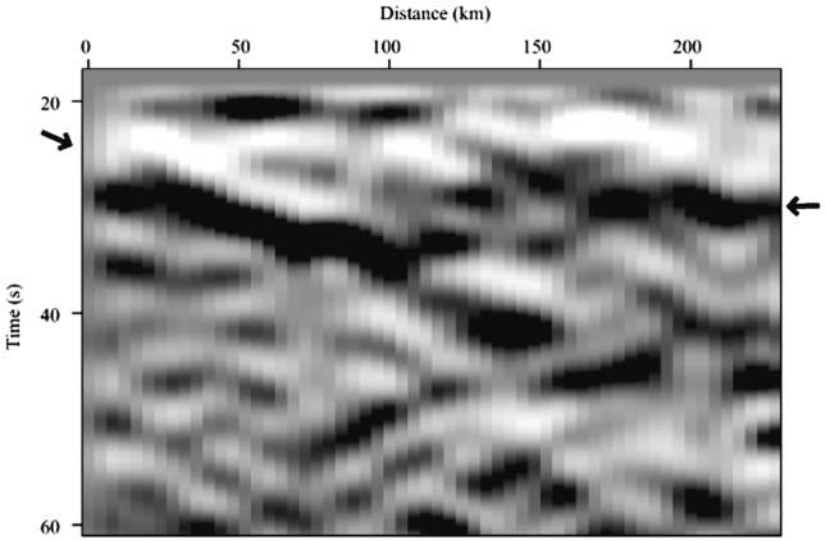

Figure 9. Image plot of the deconvolution of the processed radial component of the seismic data with the source wavelet estimated from the *SV* autocorrelation for seismic event 14. The arrow on the left edge shows the beginning of the dipping slab on the *PpPs* phase of the western margin of the continent in the Cascadia subduction zone in Oregon. The arrow on the right edge shows the approximate location of the Moho beneath the continent to the east.

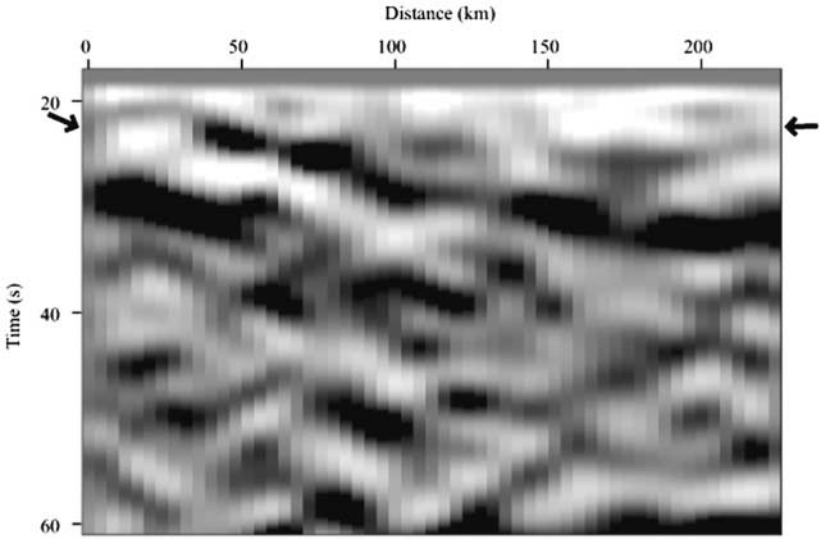

Figure 10. Image plot of the deconvolution of the processed vertical component with the estimate of the source wavelet from the *SV* autocorrelation for the individual stations. The arrow on the left edge shows the beginning of the dipping slab on the *PpPp* phase of the western margin of the continent in the Cascadia subduction zone near Oregon. The polarity of the subduction zone pulse results in a light shaded pulse for this phase. The data shown here is obtained from seismic event 5. The arrow on the right edge shows the approximate location of the Moho beneath the continent to the east.

phase estimate of the source wavelet obtained from the *SV* autocorrelation approach. The arrow on the left edge indicates the approximate location of the *PpPs* phases from the dipping slab at the western margin of the continent in the Cascadia subduction zone in Oregon. The arrow on the right edge shows the approximate location of the *PpPs* phase for the Moho beneath the continent to the east.

Figure 10 shows the image plot of seismic event 5 for the vertical component. The traces have again been interpolated to an equal spacing of 4 km prior to making the image plot using SU. Also, the direct *P* wave has been muted out at the top near 18 sec, and the traces have been filtered to less than 0.3 Hz using a zero-phase butterworth filter. Figure 10 shows the result of deconvolving the minimum-phase Z component seismograms with the estimate of the minimum-phase source wavelet obtained from the *SV* autocorrelation function for each station. The arrow on the left edge shows the approximate location of the dipping slab on the *PpPp* phase of the western margin of the continent in the Cascadia subduction zone near Oregon. The polarity of the subduction zone pulse results in a light shaded pulse for this phase. The arrow on the right edge shows the approximate location of the Moho beneath the continent of the east. This can be compared with the results of Li and Nabelek (1999) (Fig. 7) for the same event where the dip of the slab and the vertical timing compares very well. Although not as clear, the Moho beneath the eastern side of the model is indicated by the arrow on the right edge of the model.

In order to directly compare with the imaging results of Rondenay *et al.* (2001), an additional migration imaging step that converts time to depth is required and this procedure is described by Bostock *et al.* (2001). Also, these authors stacked over many events to obtain their final images. Nowack *et al.* (2006) use a Gaussian beam approach to perform

seismic imaging of the deconvolved teleseismic *P*-wave data, but here we are concerned only with the deconvolution aspects of the problem.

Conclusions

The autocorrelation of the *SV* component has been used to obtain an estimate of the source wavelet assuming that the *P* to *SV* scattering coefficients from the crust and the upper mantle are random and white. The estimated source wavelet can be used to deconvolve teleseismic *P*-wave data to obtain both *P* to *P* and *P* to *SV* scattered components. The source wavelet is not assumed to be minimum phase. However, both the seismic data and the estimated source wavelet are processed to be minimum phase prior to deconvolution. This assumes that the direct transmitted wave is larger than the scattered waves. Deconvolution using the *SV* autocorrelation function was first tested using 1D and 2D synthetic data and then using observed seismic data from the 1993 Cascadia seismic experiment.

Acknowledgments

The authors thank Michael Bostock and an anonymous reviewer for their constructive comments on the manuscript.

References

Baig, A. M., M. G. Bostock, and J.-P. Mercier (2005). Spectral reconstruction of teleseismic P Green's functions, *J. Geophys. Res.* **110,** no. B08306, doi 10.1029/2005JB003625.

Bostock, M. G. (2004). Green's functions, source signatures, and the normalization of teleseismic wave fields, *J. Geophys. Res.* **109,** no. B03303, doi 10.1029/2003JB002783.

Bostock, M. G., S. Rondenay, and J. Shragge (2001). Multiparameter two-dimensional inversion of scattered teleseismic body waves, 1, Theory for oblique incidence, *J. Geophys. Res.* **106,** 30,771–30,782.

Kennett, B. L. N. (1991). The removal of free surface interactions from the three-component seismograms, *Geophys. J. Int.* **104,** 153–163.

Langston, C. A. (1977). The effect of planar dipping structure on source and receiver responses for constant ray parameter, *Bull. Seism. Soc. Am.* **67,** 1029–1050.

Langston, C. A. (1979). Structure under Mount Rainier, Washington, inferred from teleseismic body waves, *J. Geophys. Res.* **84,** 4749–4762.

Langston, C. A., and J. K. Hammer (2001). The vertical component P-wave receiver function, *Bull. Seism. Soc. Am.* **91,** 190–201.

Li., X., and J. L. Nabelek (1999). Deconvolution of teleseismic body waves for enhancing structure beneath a seismometer array, *Bull. Seism. Soc. Am.* **89,** 190–201.

Mercier, J. P., M. Bostock, and A. Baig (2006). Improved Green's functions for passive source structure studies, *Geophysics* (in press).

Nowack, R. L., S. Dasgupta, G. T. Schuster, and J. M. Sheng (2006). Correlation migration using Gaussian beams of scattered teleseismic body waves, *Bull. Seism. Soc. Am.* **96,** 1–10.

Oppenheim, A. V., and R. W. Schafer (1975). *Digital Signal Processing*, Prentice-Hall, Englewood Cliffs, N. J.

Owens, T. J., G. Zandt, and S. R. Taylor (1984). Seismic evidence for an ancient rift beneath Cumberland Plateau, Tennessee: a detailed analysis of broadband teleseismic P-waveforms, *J. Geophys. Res.* **89,** 7783–7795.

Reading, A., B. L. N. Kennett, and M. Sambridge (2003). Improved inversion for seismic structure using transformed, S-wavevector receiver functions: removing the effects of the free surface, *Geophys. Res. Lett.* **30,** doi 10.1029/2003GL018090.

Robinson, E. A., and O. M. Osman (Editors) (1996). *Deconvolution 2*, Geophysics Reprint Series No. 17, Society of Exploratory Geophysics, Tulsa, Okla.

Rondenay, S., M. G. Bostock, and J. Shragge (2001). Multiparameter two-dimensional inversion of scattered teleseismic body waves, 3, Application to the Cascadia 1993 data set, *J. Geophys. Res.* **106,** 30,795–30,808.

Shragge, J., M. G. Bostock, and S. Rondenay (2001). Multiparameter two-dimensional inversion of scattered teleseismic body waves, 2, Numerical examples, *J. Geophys. Res.* **106,** 30,783–30,794.

Stockwell, J. W., and J. K. Cohen (2002). *The* New *SU User's Manual*, Center for Wave Phenomena, Colorado School of Mines, Golden, Colorado.

Svenningsen, L., and B. H. Jacobsen (2004). Comment on "Improved inversion for seismic structure using transformed, S-wavevector receiver functions: removing the effects of the free surface," by Anya Reading, Brian Kennett and Malcolm Sambridge, *Geophys. Res. Lett.* **31,** doi 10.1029/2004GL021413.

Vinnik, L. P. (1977). Detection of waves converted from P to SV in the mantle, *Phys. Earth Planet. Interiors* **15,** 39–45.

Webster, G. M. (Editor) (1978). *Deconvolution*, Geophysics Reprint Series No. 1, Society of Exploratory Geophysics, Tulsa, Okla.

Department of Earth and Atmosphoric Sciences
500 Stadium Mall Drive
Purdue University
West Lafayette, Indiana 47907
sdasgup@purdue.edu
nowack@purdue.edu

Manuscript received 19 December 2005.